ELSEVIER

Journal of Fluids and Structures 20 (2005) 105–127

JOURNAL OF FLUIDS AND STRUCTURES

www.elsevier.com/locate/jfs

Topological flow evolutions in cylinder of a motored engine during intake and compression strokes

R.F. Huang[a,*], C.W. Huang[a], S.B. Chang[a], H.S. Yang[a], T.W. Lin[a], W.Y. Hsu[b]

[a]*Department of Mechanical Engineering, National Taiwan University of Science and Technology, 43 Keelung Road, Section 4, Taipei, Taiwan, ROC*

[b]*Department of Research and Development, Kwang Yang Motors, 35 Wan Hsing St., Kaohsiung, Taiwan, ROC*

Received 16 January 2004; accepted 29 September 2004
Available online 4 January 2005

Abstract

The evolution processes of the in-cylinder flows in the axial and diametral planes of a motored two-valve, single-cylinder, four-stroke engine during the intake and compression strokes are diagnosed by using a particle image velocimeter. A device, which is called the "inlet deflection-valve", being capable of deflecting the inlet flow is installed upstream of the inlet port. The engine cylinder, piston, and accessories are modified to meet the requirements of laser-light sheet shooting and camera viewing when the particle image velocimetry is applied. A conditional sampling technique is employed to acquire the instantaneous velocity data at predetermined crank angles. Ensemble averages of large amounts of the instantaneous velocity maps obtained at various crank angles present clear pictures of the evolution processes of the tumble and swirl motions in the engine cylinder. Sectional streamlines and the velocity vectors show the topological flow structures. The inception, establishment, evolution, and destruction processes of the swirling and tumbling vortical structures during the intake and compression strokes are presented and discussed. Quantified strengths of the rotating motions in the axial and diametral planes are presented by dimensionless tumble-and-swirl ratios, which are defined as the ratio of the mean angular velocity of the vortices in the target plane at a certain crank angle divided by the average crank angle velocity. By using the quantified nondimensional parameters, the correlation between the in-cylinder flow motions and the engine performance is analyzed and discussed.

1. Introduction

The fluid motions inside the cylinder of an internal combustion engine strongly influence the performance of the engine. By optimizing combustion with enhanced in-cylinder flow motions and by means of charge stratification achieved through gasoline direct injection technique, the lean operating combustion limit can be significantly extended and the emissions of pollutants can be reduced (Iwamoto et al., 1997; Arcoumanis et al., 1998). It is well known that the structure of the turbulent flow field is a determining factor in the initiation, the rate of propagation, and the efficiency of the combustion process in an internal combustion engine (Rask, 1979). Experiments have shown convincingly that, in engines without significant squish regions, the turbulence structure during entire cycle is determined by the vortical flows which are induced by the inducted inlet flows during intake stroke (Rask, 1979).

*Corresponding author. Tel.: +886 2 2737 6488; fax: +886 2 2737 6460.
E-mail address: rfhuang@mail.ntust.edu.tw (R.F. Huang).

0889-9746/$ - see front matter © 2004 Elsevier Ltd. All rights reserved.
doi:10.1016/j.jfluidstructs.2004.09.002

Nomenclature

B	bore of engine cylinder
CA	crank angle of engine
C_{HC}	hydro-carbon concentration of engine exhaust
L	lift of valve
N	engine speed, rpm
n	total number of grid points in target plane
P	engine power
R_X	coordinate in diametral direction parallel to X coordinate in image plane for swirl motion
R_Z	coordinate in diametral direction normal to X coordinate in image plane for swirl motion
S	stroke of the piston motion
SFC	specific fuel consumption of engine
$S_{v,CA}$	swirl ratio
$\overline{S_{v,CA}}$	cycle-averaged swirl ratio
T	torque output of engine
$T_{v,CA}$	tumble ratio
$\overline{T_{v,CA}}$	cycle-averaged tumble ratio
u	velocity component in X direction
v	velocity component in Y direction
X	coordinate in diametral direction on image plane for tumble motion
Y	coordinate in axial direction on image plane for tumble motion
Φ	open angle of inlet deflection valve
ω	angular speed of crank shaft

When inducted through the specially designed intake port and valve, the intake flow behaves like a swirling or non swirling annular jet, interacts with the cylinder wall, and creates large scale rotating flow patterns within the cylinder. The primary in-cylinder large scale rotating flows set up by the conical intake jet may in general be characterized into two categories: the swirl motion rotating about the cylinder axis and the tumble motion rotating about the diametral axis (Heywood, 1987). It is becoming clear that generating a significant vortical flow motion inside the engine cylinder (swirl and/or tumble motions) during the intake process is one of the more promising ways to obtain high turbulence intensity eventually in the late stroke of compression and achieve a fast burning rate (Heywood, 1988). A well-defined swirl and/or tumble flow structure is more stable than other large scale in-cylinder flows and, therefore, it may break up later in the cycle, giving higher turbulence during combustion (Heywood, 1987, 1988). Therefore, a good understanding of the evolution process of fluid motion in internal combustion engines is critical to develop engine designs with the most attractive operating and emission characteristics.

The in-cylinder flow characteristics have been studied by many investigators. Ekchian and Hoult (1979) applied a flow visualization technique to a water-analogy apparatus and obtained streak flow patterns of bulk flow in the axial plane of a transparent cylinder with an inlet valve located at the center of the cylinder head. The results displayed an evolution process of a pair of counter-rotating vortices during the intake cycle (Ekchian and Hoult, 1979). The turbulence properties were measured by Hirotomi et al. (1981), Arcoumanis et al. (1982), Liou and Santavicca (1985), and Nadarajah et al. (1998) by using laser Doppler anemometers (LDV). Some evidence suggested that large turbulence intensities were primarily induced by the shear effects of the inducted jet and the vortical flow motions evolved during the engine cycles. The detailed evolution process of the in-cylinder flows, however, was not intensively studied, partly because of the insufficiency of the measuring instrumentation.

More recently, time-evolving in-cylinder flow structure attracted the attention of investigators, because of the mature development of the particle image velocimetry (PIV) (Raffer et al., 1998; Adrian, 1991). Khalighi (1991) employed a particle tracking velocimeter (PTV) to study the intake tumble motion of a four-valve, single-cylinder engine with shrouded intake valves in a water analogy. The velocity vector field of the tumble motion at a certain instance was successfully measured. The streak evolution process of the vortical flow structure, however, was not shown. Lee and Farrel (1993) and Valentino et al. (1993) employed PIV to measure the steady and unsteady flow patterns around the intake valve for a four-valve diesel engine. The jet characteristics of the induced flows and corner vortex in the cylinder were validated. The evolution process of the in-cylinder flow structures was not addressed. Recently, a PIV system was utilized by Jackson et al. (1997) in the water analogy rig of a simulated engine to examine the correlation between the tumble flow motions and the combustion characteristics of the real engine. Results show that the dynamic water flow rig provides improved correlation with combustion data, compared to that obtained with conventional steady flow methods for characterizing in-cylinder flow patterns. Freek et al. (1998) used film-PIV to examine the cycle-by-cycle variation of swirl flow motion in a five-valve motored engine cylinder. The temporal evolution of the in-cylinder flow was presented. Rouland et al. (1998) presented the velocity vector fields of the in-cylinder tumble motion of a motored four-valve engine. They found that the engine speed did not really modify the tumble intensity. The PIV technique has also been applied to detect the internal structure of the diesel fuel spray (Cao et al., 2000).

The purpose of this work is to unveil the time-evolving process of the flow in the engine cylinder during the intake and compression strokes of a two-valve single-cylinder engine, with and without deflected inlet flow by using a two-dimensional PIV. Instantaneous and cycle-averaged intensities of the tumble and swirl flow motions are quantified by calculating the dynamically- defined flow parameters, the tumble ratio and the swirl number, respectively. The engine performance is measured and cross-analyzed with the quantitatively expressed tumble ratio and swirl number. Correlations between the parameters of the vortical flow motions are sought and discussed.

2. Experimental system

2.1. Test rig

A four-stroke, single-cylinder engine for a motorbike is used for the study of the flows in the engine cylinder. The bore B is 52.4 mm, the stroke S is 57.8 mm, and the displacement is 124.6 cm^3/stroke. The shape of the cylinder head is hemispherical on the top of the combustion chamber. The inlet and exhaust valves are arranged on opposite sides of the central axis, as shown in Fig. 1. The diameter of the inlet and exhaust valve is 27.5 and 23.5 mm, respectively. The maximum lift of the inlet and exhaust valve is 7.25 and 6.85 mm, respectively. Movements of the valves are driven by a single overhead camshaft (SOHC). The inlet valve opens at 30° crank angle before top dead center and closes at 80°

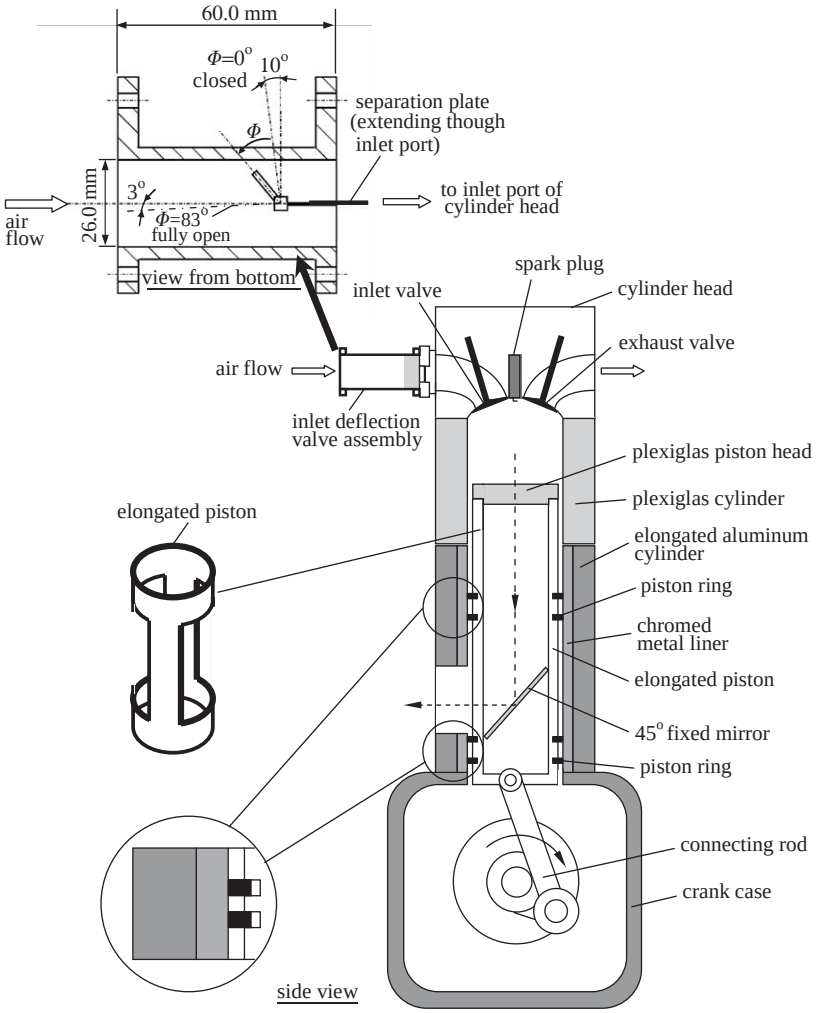

Fig. 1. Modified engine for PIV measurements.

crank angle after bottom dead center. The exhaust valve opens at 45° crank angle before bottom dead center, and it closes at 45° after top dead center. The valve-lift profiles of the inlet and exhaust valves are shown in Fig. 2. The angle between the central axis of the inlet valve and the symmetry axis of the cylinder is 20°. The angle between the inlet port and the symmetry axis of the cylinder is 65°.

The engine is modified to fit the requirements of the PIV measurements, as shown in Fig. 1. The original metal cylinder is replaced by a transparent cylinder which is made of Plexiglas so that the laser-light sheet can penetrate through the cylinder wall and the camera can see the image plane through the cylinder when the tumble motion is to be detected. A section of aluminum cylinder with chromed metal liner is inserted in-between the Plexiglas cylinder and the crank case. The original piston is also replaced by an elongated hollow cylindrical aluminum frame, as shown in the subset of Fig. 1. The top end of the elongated piston frame is screwed with a Plexiglas-made circular disc which serves as the piston head. The bottom end of the elongated piston frame is bearing-connected to the original connecting rod so that the original stroke of the piston motion is not changed. Four piston rings are inserted between the elongated piston and the cylinder at specially arranged locations to reduce the blowby of air and the slapping of elongated piston. An elliptic mirror is inserted in the space of the elongated piston frame and fixed onto the aluminum cylinder at 45° with the axis. The mirror does not have any contact with the piston frame, so that it will not be affected by the motion of the piston. The mirror is used to reflect the particle images in diametral planes illuminated by the laser-light sheets when the swirl motion is to be detected. The aluminum cylinder has an opening so that the camera can picture the reflected image from the 45°-mounted mirror.

An inlet deflection-valve assembly, as shown in the detail in Fig. 1, is connected to the inlet port to modify the inlet flows before entering the cylinder. The hinge of the deflection valve is located on the central axis of the passageway of round cross-section. Downstream the hinge of the deflection valve, a separation plate is attached all the way through the inlet port along the bisection plane. The deflection valve has a threshold of 10° from the diametral plane when it is closed and is approximately 3° passing over the central plane of the passage when it is fully open. The open angle Φ of the deflection valve denotes the angle between the valve plane and the threshold plane. For example, $\Phi = 0°$ stands for the valve closed and most of the air-flow allowed to pass through the un-blocked side of the passage. When $\Phi = 83°$, the valve is fully open at its geometric limit; in this situation the flow which go into the left and right passageways which are separated by the separation plate are a little unbalanced, because the cross-sectional areas of the left and right passageways are slightly different by the 3° over-deviation of the deflection-valve from the central plane.

During the intake stroke, the top dead center (TDC) of the piston is taken as 0° of the crank angle, and the bottom dead center (BDC) is 180°. The compression stroke starts from CA = 180° to 360°. The instantaneous crank angle is indicated by output signals of an encoder which is mounted to the crank axis, as shown in Fig. 3. In order to install the encoder at the proper and accurate position, a specially designed gauge and electronic indicators are employed to precisely locate the BDC position. The encoder is RG-360-05 made by IHI Co., with a resolution of one degree CA. The Z and A signals of the encoder outputs are used to indicate the BDC and crank angles, respectively, and also serve as the trigger signals to the electronic synchronizers.

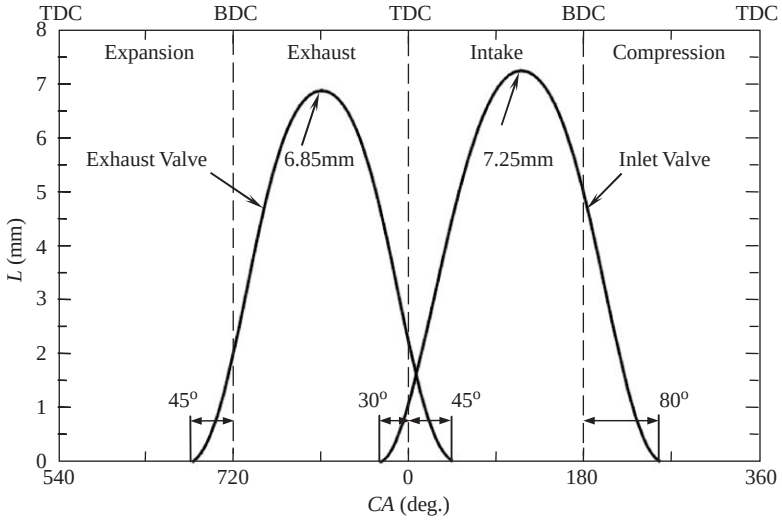

Fig. 2. Valve-lift profiles of inlet and exhaust valves.

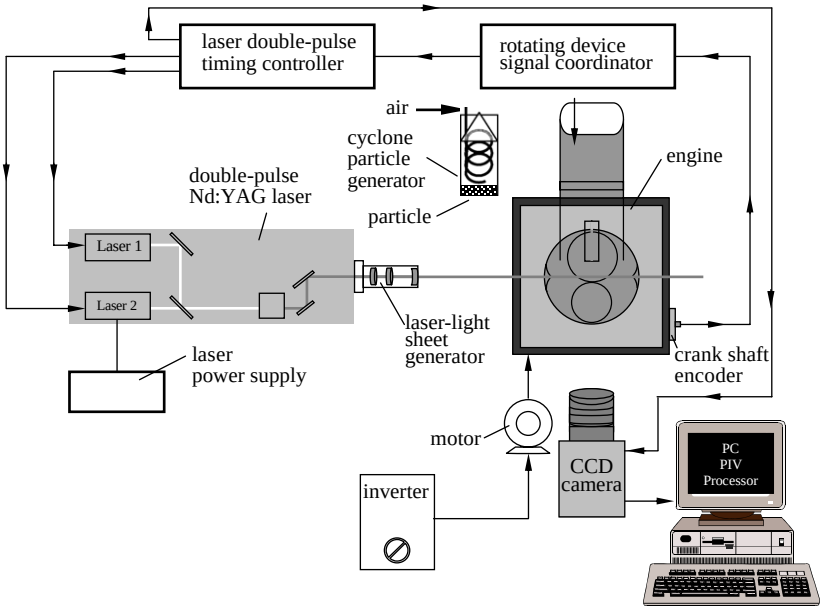

Fig. 3. Experimental setup.

The engine is driven by an electric motor of 10 HP through a set of rubber coupling and connecting mechanism. The rotating speed of the motor is controlled by a low noise-emitting inverter, which can drive the engine speed between 0 and 7200 rpm. The whole modified engine is mounted on a specially designed anti-vibration test rig. The maximum vibration amplitudes at the engine speed of 1500 rpm in the axial and lateral directions are 1 and 3 μm, respectively. In terms of camera resolution which will be discussed in the following paragraphs, these vibration amplitudes correspond to about 0.02 and 0.06 pixels only and make little influence on the measurement accuracy. All measurements in this study are performed at the engine speed $N = 1500$ rpm.

Plastic particles made of polyamide are seeded into the engine through a cyclone particle generator as described by Glass and Kennedy (1978) to scatter the laser light. The diameters of particles are between 30 and 50 μm and the specific weight is 1.03 at 25 °C. Considering the effect of turbulent diffusion, the particles are estimated to be capable of following fluctuating frequencies up to 3 kHz, according to Mei's method (Mei, 1996).

2.2. PIV system and interrogation analysis

The PIV system includes a double-pulse Nd:YAG laser, a CCD camera, and a home-made electronic controller consisting of a "rotating-device signal coordinator" and a "laser double-pulse timing controller," as shown in Fig. 3.

2.2.1. Pulsing lasers

Two independently controllable pulsing lasers are packed in one casing for the purpose of generating consecutive double-pulses. Alignment optics is installed in the casing, so that collimation of the light paths of the double pulsed laser beams is easily accessed. The laser employs flash-lamp-pumped Nd:YAG rod in a thermally compensated resonator to generate radiation at 1064 nm via an IR head. The 1064 nm laser pulse is conducted through an optical attenuator which consists of a half-wave plate and a polarizer to control the laser energy without affecting the beam quality. The second harmonic at 532 nm is then generated by passing the IR beam through an angle tuned KTP crystal. Energizing and lasing of the lasers are controlled by external triggering of the pumping flash-lamp and the Q-switch, respectively. The control signals are TTL compatible which are supplied by home-made electronic controllers. The time separation between lamp-energizing and Q-switch triggering signals is optimized to be about 25 μs in this study. The laser pulse emits at 180 ns after the Q-switch signal is triggered. The maximum pulsing rate is 30 double-pulses per second. The maximum pulsing energy is 90 mJ. The pulse width is between 3 and 5 ns. The jittering is ± 0.5 ns. The green light beams at 532 nm leaving the laser head are expanded as a 20° light sheet through a laser-light sheet generator which is installed at the exit of the laser-head. The thickness of laser-light sheet is adjusted to about 0.5 mm.

2.2.2. Camera and image grabbing

The particle images are recorded by a Roper Scientific's Megaplus Model ES 1.0 CCD camera. The resolution is 1008×1018 pixels. The pixels are $9\,\mu m^2$ and can be operated continuously or in an external trigger mode. The pixel array is zoomed and mapped to a physical region of approximately 45 mm so that the spatial resolution is about 45 μm/pixel. The external trigger mode is used in this study by applying the timing-controlled trigger signal from the electronic controller. The camera has an output channel data rate of 20 MHz, which offers a maximum frame rate of 30 frames per second. Exposure times of 0.125–33 ms are possible with the camera's electronic shutter. A "triggered double exposure mode" (frame straddling technique) facilitates the application of PIV. When operated at frame straddling mode, the maximum framing rate turns out to be 15 pairs per second.

In this study, the image pairs are taken every four engine revolutions so that the framing rate is reduced down to 6.25 pairs per second when the engine is motored at 1500 rpm. Totally, four hundred image pairs are taken and stored in the computer memory for each run of experiment. Two consecutive images with properly pre-set exposure times are transferred at one operation of electronic shutter. Timing of the double-pulse laser-light sheet illuminations is set via the electronic controllers so that they fall into each exposure period of the image pairs. The separation time between consecutive laser pulses is set to 25 μs by using the electronic controllers. The experiments are conducted in the dark so that the effective exposure time is controlled by the laser pulse width, i.e., 3–5 ns. The frame grabber is an EPIX's PIXCID Imaging Board which is operated by software of XCAP-Plus. The images are transferred and stored in the computer memories of 2 GB. Each image occupies about 2 MB so that the system can take at most 500 image pairs at one operation.

2.2.3. Electronic synchronizers

The electronic control system consists of two parts: the "rotating-device signal coordinator" and the "laser double-pulse timing controller". The "rotating-device signal coordinator" receives series of TTL-compatible signals from an encoder which is mounted on the crank-shaft of the engine. Functions like "number of leading-revolutions to skip", "number of revolutions for outputting one signal", "crank angle for outputting one signal", and "total number of output signals" are built-in, so that the technique of conditional sampling can be used. The TTL-compatible output signals of the "rotating-device signal coordinator" are fed to the "laser double-pulse timing controller" according to the timing settings. The "laser double-pulse timing controller" bears the functions of outputting TTL signals to control the timings for flashing of the lasers and shuttering of the camera. Time separations between the triggering signals of "rotating-device signal coordinator" and the lamping, the lamping and the Q-switching, as well as the first lamping and the second lamping are flexibly adjustable. Time separation between consecutive flashes of the lasers can be easily set between 0 and 9999 μs at a resolution of 0.1 μs.

2.2.4. Interrogation analysis

Two consecutive image frames are analyzed by using the cross-correlation technique (Keane and Adrian, 1992) imbedded in the software of VidPIV4 which is obtained from the Optical Flow Systems. The software calculates the average displacement of local groups of particles in consecutive images. The interrogation window is set to 32×32 pixels. The displacement of the double-exposed images relative to the length of the interrogation area is held to be smaller than 1/4 as suggested by Keane and Adrian (1990) to reduce velocity bias in the regions of large velocity gradients. The seeding density is adjusted to keep the number of particle-image pairs per interrogation spot no less than four so that the measurement reliability would not become significantly poor (Keane and Adrian, 1990). The percentage of outliers in a vector-map usually depend on factors such as seeding density, seeding homogeneity, out-of-plane motion, pulse separation, and analysis parameters such as the size of interrogation area. Even for well-optimized PIV images which are analyzed with appropriate parameters, there is still a finite probability of getting some outliers. Filtering and interpolation are used to identify outliers and then regenerate missing values. A global filter is used to discriminate outliers from valid vector values by comparing how close each vector component is to the mean of the vector-values across the whole vector-map. A local filtering performs a similar comparison procedure by using the nearest neighbors, rather than all the values in the vector-map to gain information of the spread of values. The global filter finds all the globally inconsistent values while the local filter finds those that may be globally consistent but not smoothly consistent with the local variations in vector magnitude and direction. In general, less than 15% of spurious vectors per instantaneous field are observed in this study. More than 2300 instantaneous velocity vectors are obtained from the present PIV images. The general-purpose interpolation kernel, which uses nearest 8 or 24 neighbor values for processing, is optimized for vector-maps with a 50% overlap of the interrogation and the interpolation algorithm. The method of interpolation is based on a weighted mean technique which replaces the values at filtered sites in an iterative manner by replacing those with the most surrounding valid values first, then working toward those that are less favorably positioned for accurate and reliable interpolation. Adaptive cross-correlation employing smaller

interrogation size and smaller grid spacing is finally applied to the vector field which is generated from the regular procedure of cross-correlation, filtering, and interpolation to provide higher resolution and accuracy than the first pass (Keane et al., 1995; Hart, 1999).

3. Results and discussion

The view planes for detections of tumble and swirl motions are defined in Fig. 4. For tumble motion measurement, the axial plane cutting through the inlet and exhaust valves is illuminated by the laser-light sheet, and the camera is arranged to face to the plane at an angle of 90°. The physical range of view is $4.6 \times 4.6\,\mathrm{cm}^2$. The coordinates in the diametral and axial directions are denoted by X and Y, respectively. The origin is placed at the left-lower limit of the view plane. For swirl motion measurement, the laser-light sheet is illuminated across several diametral planes at several axial stages. The particle images across the target plane are transported through the transparent piston head, reflected by the mirror mounted at an angle of 45° in the elongated hollow cylindrical aluminum frame, as mentioned in the previous section, and finally focused by the camera lens. The physical range of view is a circular plane of diameter 4.3 cm, which is limited by the piston geometry. The coordinate system for the description of the swirl motion is denoted by (R_X, R_Z), as shown in Fig. 4. The origin is located at the center of the cylinder.

3.1. Flow evolution in symmetry plane

3.1.1. Inlet deflection-valve closed ($\Phi = 0°$)

All the data presented in Figs. 5–12 are obtained from the ensemble average over 100 instantaneous data maps. It is found in this work that the ensemble average gained by using more than 40 data maps will yield almost identical flow patterns and velocity vectors.

Fig. 5 shows the evolution process of the in-cylinder flows in the symmetry plane during intake stroke when the inlet deflection-valve is closed. Velocity vectors and corresponding streamline patterns are shown in the plots. The streamlines are obtained by using the shooting method. The shooting method starts from an initial velocity vector, extends the vector to an interpolated point of the next row of vectors, interpolates the velocity vector at that point, and

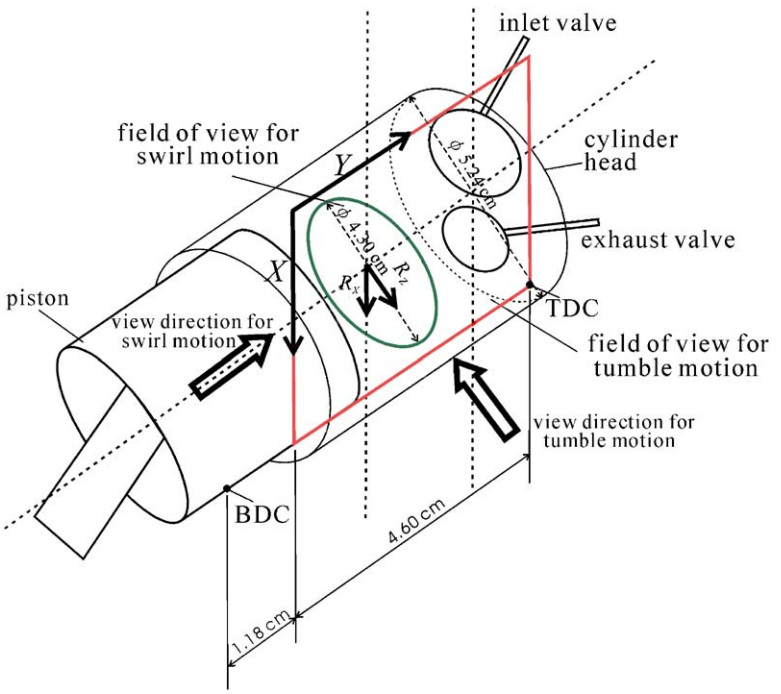

Fig. 4. Image planes and coordinate systems for detection of tumble and swirl motions.

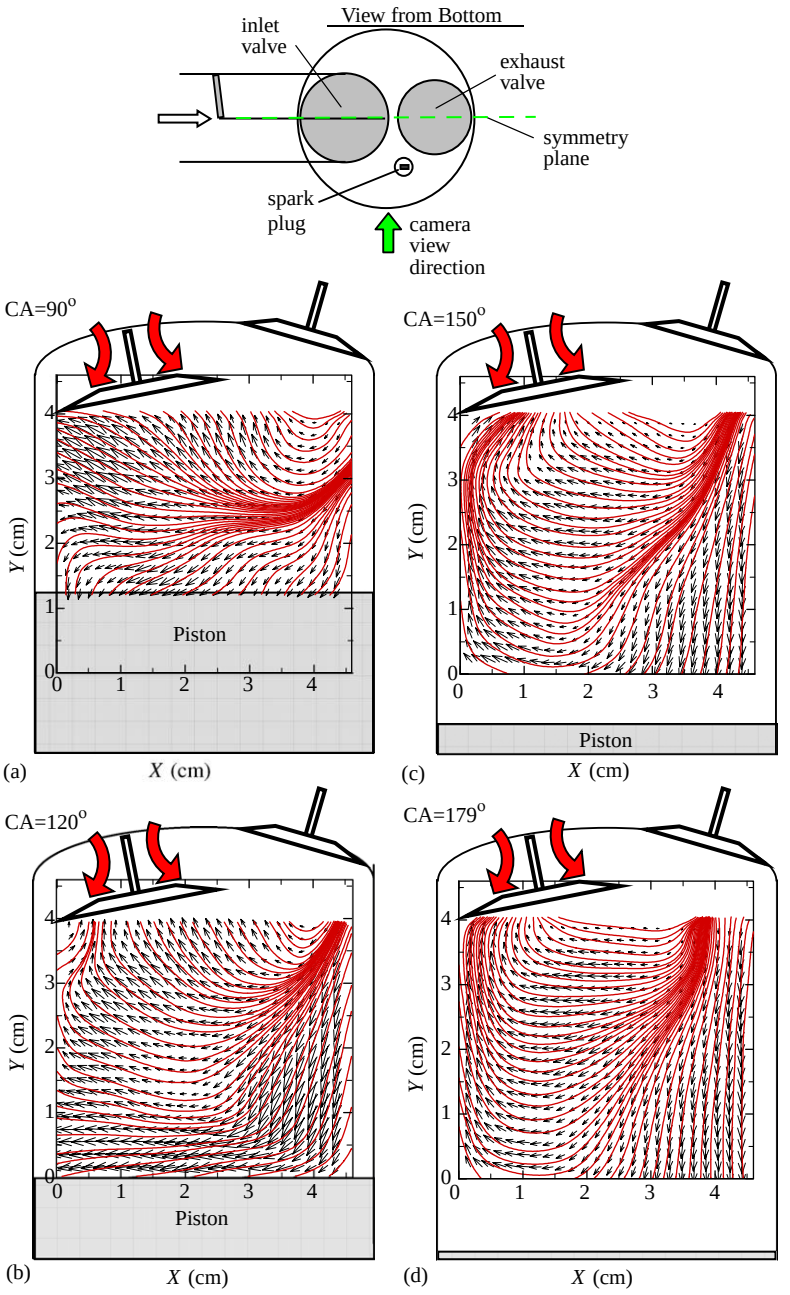

Fig. 5. Evolution of tumble flow motions during intake stroke in symmetry axial plane. Inlet deflection-valve closed ($\Phi = 0^\circ$). Engine speed $N = 1500$ rpm. Velocity data are ensemble-averaged from 100 instantaneous measurements.

proceeds to the next row of vectors. Connecting all the located points would provide the streamline. If the distance between neighboring rows is short, the streamlines obtained by this method would be smooth and accurate enough within a satisfactory accuracy. The inlet deflection-valve is closed ($\Phi = 0^\circ$), so that the inlet stream is artificially deflected. When the inlet valve is open, the air is drawn by the downward motion of the piston. It passes over the inlet valve and forms an annular jet. The annular jet expands in the engine cylinder, interacts with the cylinder walls, the piston head, and the inlet valve.

At crank angle CA $= 90^\circ$, as shown in Fig. 5(a), the jet flows going through the inlet valve expand and impinge directly on the right cylinder wall. The velocity vectors going from the valve edge are not shown because the

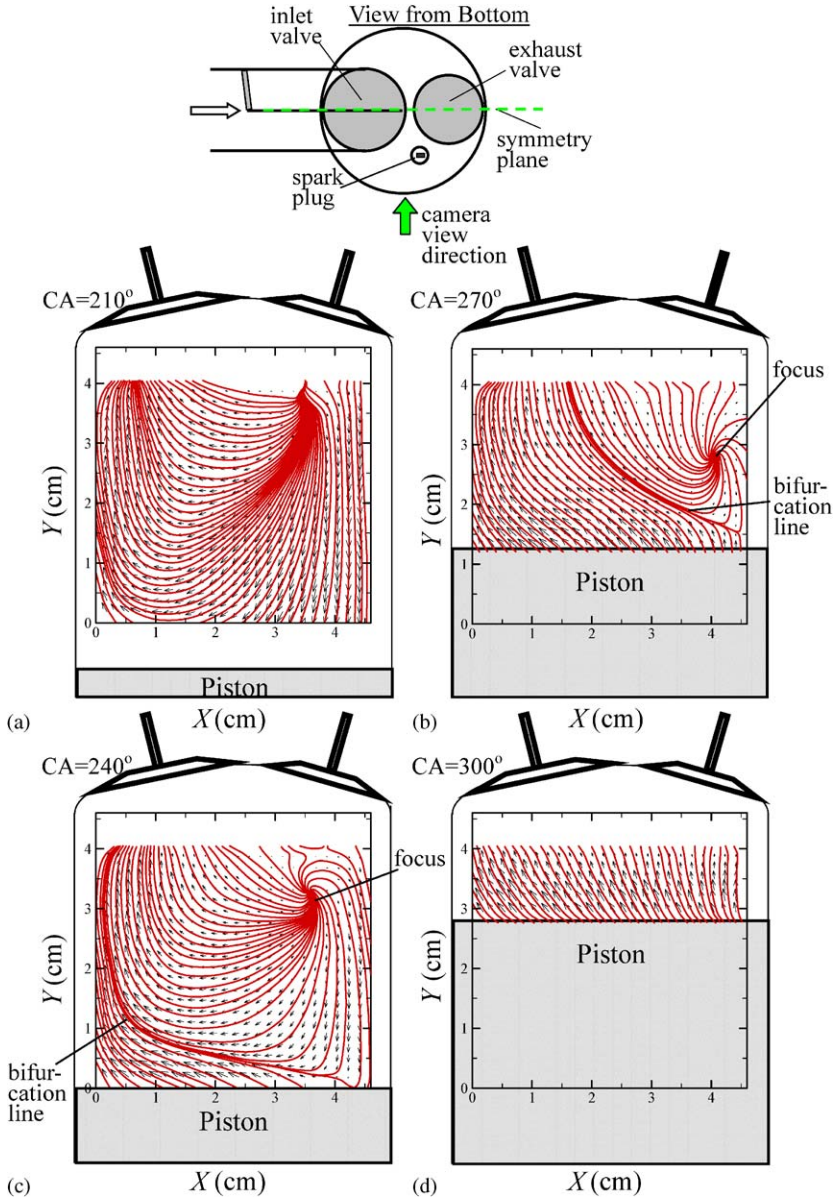

Fig. 6. Evolution of tumble flow motions during compression stroke in symmetry axial plane. Inlet deflection-valve closed ($\Phi = 0^\circ$). Engine speed $N = 1500$ rpm. Velocity data are ensemble-averaged from 100 instantaneous measurements.

measurement window does not cover that region. Part of the flow goes downward along the right cylinder wall and impinges on the piston head. The piston is moving downward and drawing the flow with its face velocity, so that the velocity vectors located a little above the piston head are pointing downward. Part of the right wall-impinging flow makes a turn and moves up toward the inlet valve. According to previous investigations (e.g., Huang and Lin, 1994, 1997; Huang and Tsai, 2001a,b; Huang and Yen, 2003), when a nonswirl or swirl flow passes over a disc-type bluff body, a recirculation zone (nonswirling flow) or a swirling bubble system (swirling flow) would be formed in the near wake region of the bluff body. The flows in the recirculation zone are reversed in direction and point toward the bluff body due to the sub-atmospheric pressure generated in the wake of the inlet valve. The inlet valve acts as a bluff body in this flow field. It is not surprising that a sub-atmospheric pressure is generated in the downstream area of the valve and induces reverse flows going toward the valve surface. With the reversal of the flow behind the valve face, a clockwise-

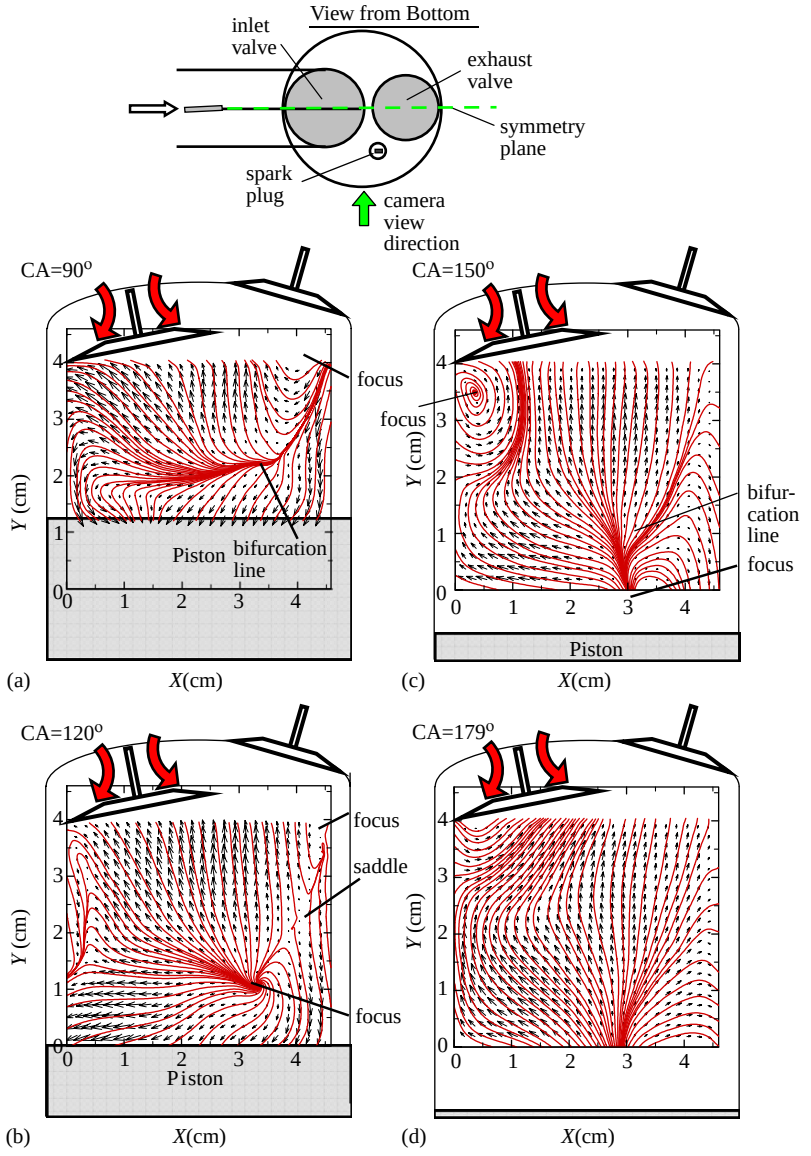

Fig. 7. Evolution of swirl flow motions during intake stroke in symmetry axial plane. Inlet deflection-valve fully open ($\Phi = 83^\circ$). Engine speed $N = 1500$ rpm. Velocity data are ensemble-averaged from 100 instantaneous measurements.

rotating recirculation structure is formed in the right upper region of the cylinder. Because the inlet valve at this crank angle is not wide open, the inlet flow going through the left side of the inlet valve is not strong. The flow pattern in the left upper corner therefore does not display influence by the flow going through the left of the inlet valve. In the region near the left lower corner, the velocity vectors point downward because the induction effect of the downward face velocity of the piston head is large at this instant.

With the downward motion of the piston, the primary features of the flow pattern in Fig. 5(a) are generally magnified in space, as shown in Fig. 5(b) for crank angle CA = 120°, except that in the regions near the left upper and lower corners. At this instant, the valve lift is large, so that the influence of the jet flow going through the left part of the inlet valve becomes obvious: the jet impinges on the left cylinder wall, turns downward, meets the upward flow of the clockwise-rotating primary vortex at $Y \approx 3$ cm, and turns upward to form a small counter-clockwise-rotating vortex around the left upper corner because of the reasoning of flow topology (Perry and Fairlie, 1974; Chong and Perry,

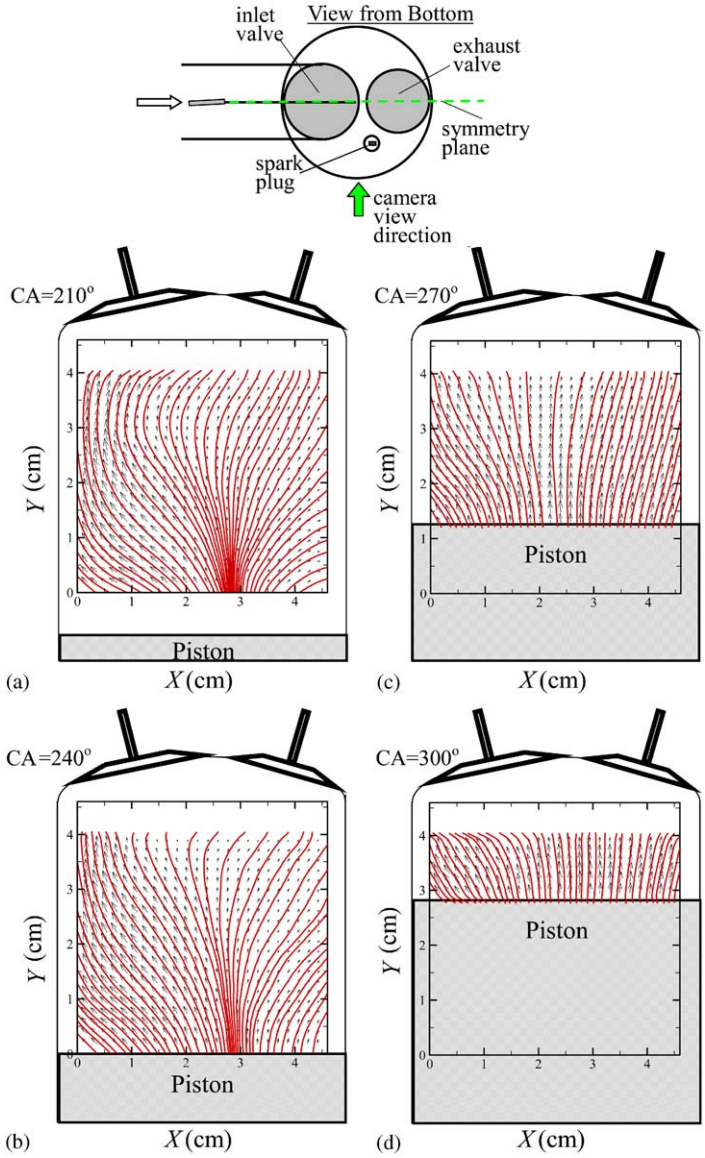

Fig. 8. Evolution of tumble flow motions during compression stroke in symmetry axial plane. Inlet deflection-valve fully open ($\Phi = 83^\circ$). Engine speed $N = 1500$ rpm. Velocity data are ensemble-averaged from 100 instantaneous measurements.

1990). The downward flow in the region near the left lower corner which is induced by the downward motion of the piston shown in Fig. 5(a) does not appear in Fig. 5(b). That may be partly caused by the decrease of the instantaneous piston velocity and the increase in strength of the clockwise-rotating vortex. The instantaneous piston velocity increases from zero to the maximum when the piston moves from the top dead center (CA = 0°) to approximately CA = 90°, and decelerates to zero when the piston reaches the bottom dead center (CA = 180°).

At CA = 150° and 179°, as shown in Figs. 5(c) and (d), the counter-clockwise-rotating vortex around the left upper corner appearing in Fig. 5(b) is not seen, because the opening of the inlet valve decreases. A structured ''tumbling'' vortex is formed in the cylinder in this central symmetry plane.

In the initial period of the compression stroke, as shown in Fig. 6(a) for CA = 210°, the features of the structured tumbling vortex remain similar to those are seen in Figs. 5(c) and (d). The piston moves upward at a small velocity during this initial period of compression stroke.

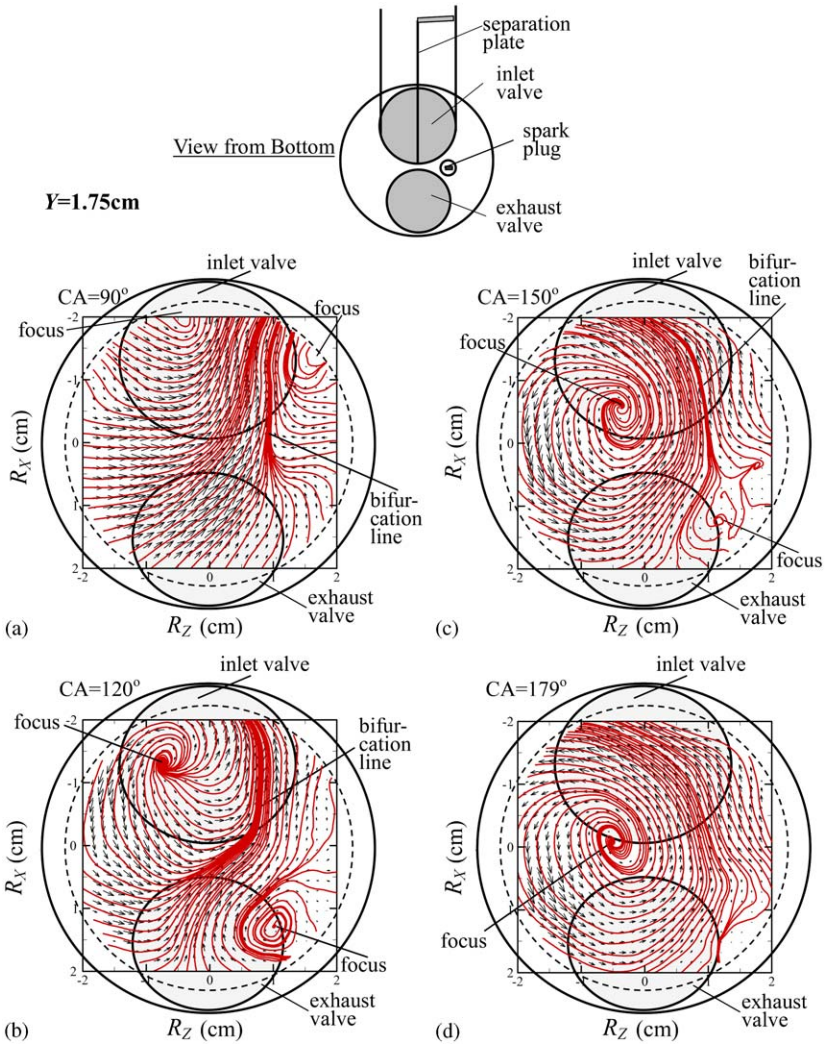

Fig. 9. Evolution of swirl flow motions during intake stroke in diametral plane $Y = 1.75$ cm. Inlet deflection-valve closed ($\Phi = 0^\circ$). Engine speed $N = 1500$ rpm. Velocity data are ensemble-averaged from 100 instantaneous measurements.

In Fig. 6(b) for CA = 240°, with the increase of the crank angle the upward velocity of the piston motion becomes large, so that the velocity vectors above and near the piston head present positive Y components. The upward flows meet the downward stream of the primary clockwise-rotating vortex, merge together, and form a left-pointing "negative open bifurcation line" (Hunt et al., 1978). A lateral vortex stretching (Tritton, 1988) in the $\pm Z$ direction is accompanied with the compression effect in the Y direction, so that a "stable focus" (Hunt et al., 1978) is formed in the right upper region of the primary vortex. This indicates that lateral vortex stretching is developed and the three-dimensional flow structure is promoted by the compression motion of the piston; thus the cascade of the turbulence kinetic energy should be enhanced subsequently (Tennekes and Lumley, 1972). In Fig. 6(c) for CA = 270°, the effect of push-up motion of the piston reduces the size of the primary counter-rotating vortex. The up-flush flows which are induced by the push-up motion of the piston increase with the increase of the piston upward velocity. The "negative open bifurcation line" thus moves from the left lower part of the cylinder (Fig. 6(b)) to the right upper part (Fig 6(c)). The primary vortex therefore shrinks to a smaller size at CA = 270°.

At the final stage of the compression stroke, as shown in Fig. 6(d) for CA = 300°, most of the kinetic energy of the rotating flow is dissipated by the viscosity due to the suspension of inlet source (Tennekes and Lumley, 1972).

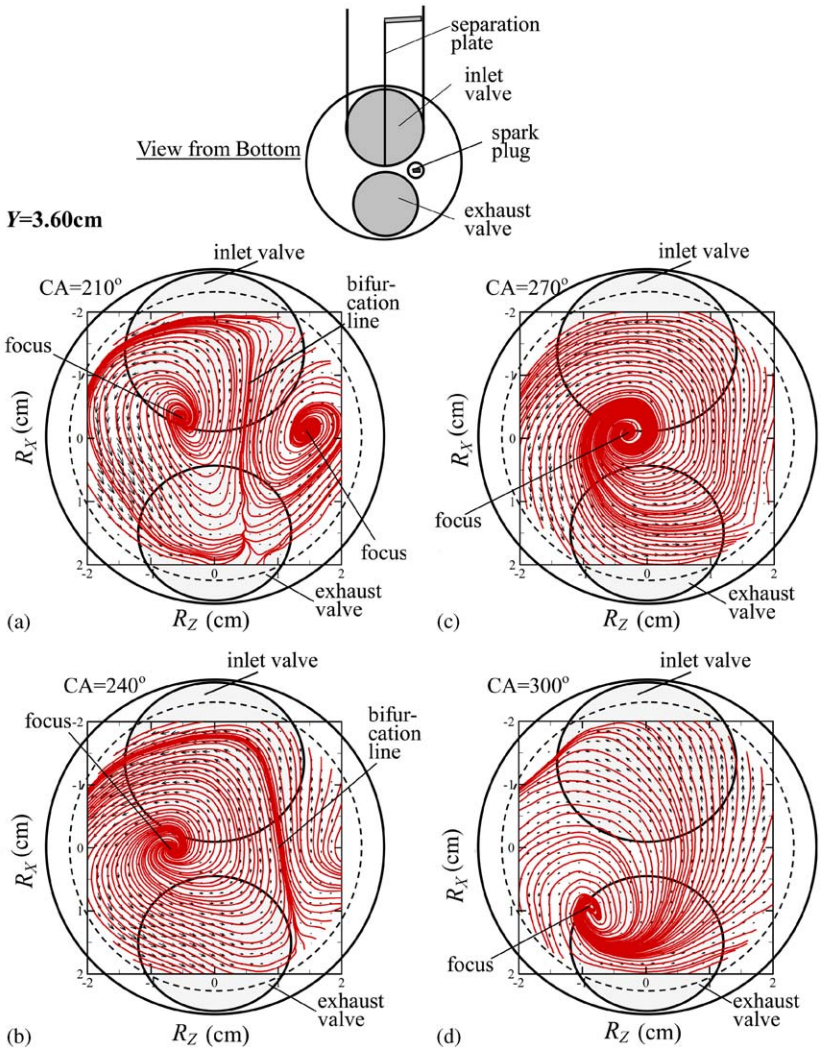

Fig. 10. Evolution of swirl flow motions during compression stroke in diametral plane $Y = 3.6$ cm. Inlet deflection-valve closed ($\Phi = 0°$). Engine speed $N = 1500$ rpm. Velocity data are ensemble-averaged from 100 instantaneous measurements.

Therefore, the flow in the cylinder is dominated by the upward motion of the piston. The upward flow velocities near the piston head are larger than those near the cylinder head.

3.1.2. Inlet deflection-valve fully open ($\Phi = 83°$)

Figs. 7 and 8 show the evolution processes of the in-cylinder flows in the symmetry plane during intake and compression strokes, respectively, when the inlet deflection-valve is fully open ($\Phi = 83°$). Because the deflection-valve has a 3° deviation from the central plane of the passage when it is fully open (as described in the previous section), the inlet stream is deflected a little by the deflection-valve in the opposite direction to the case of the deflection valve is closed. Therefore, the flows going through the passageways, which are separated by the inlet valve and the separation plate, are a little unbalanced.

At CA = 90°, as shown in Fig. 7(a), the features of flow pattern look similar to that of Fig. 5(a). However, the flow patterns become significantly different from the vortical motions in the case of $\Phi = 0°$ as the flow further evolves with the increase of crank angle. At CA = 120°, two topological critical points (Perry and Fairlie, 1974) appear. An "unstable focus" located around the right lower region of Fig. 7(b) is induced by the effect of lateral vortex stretching

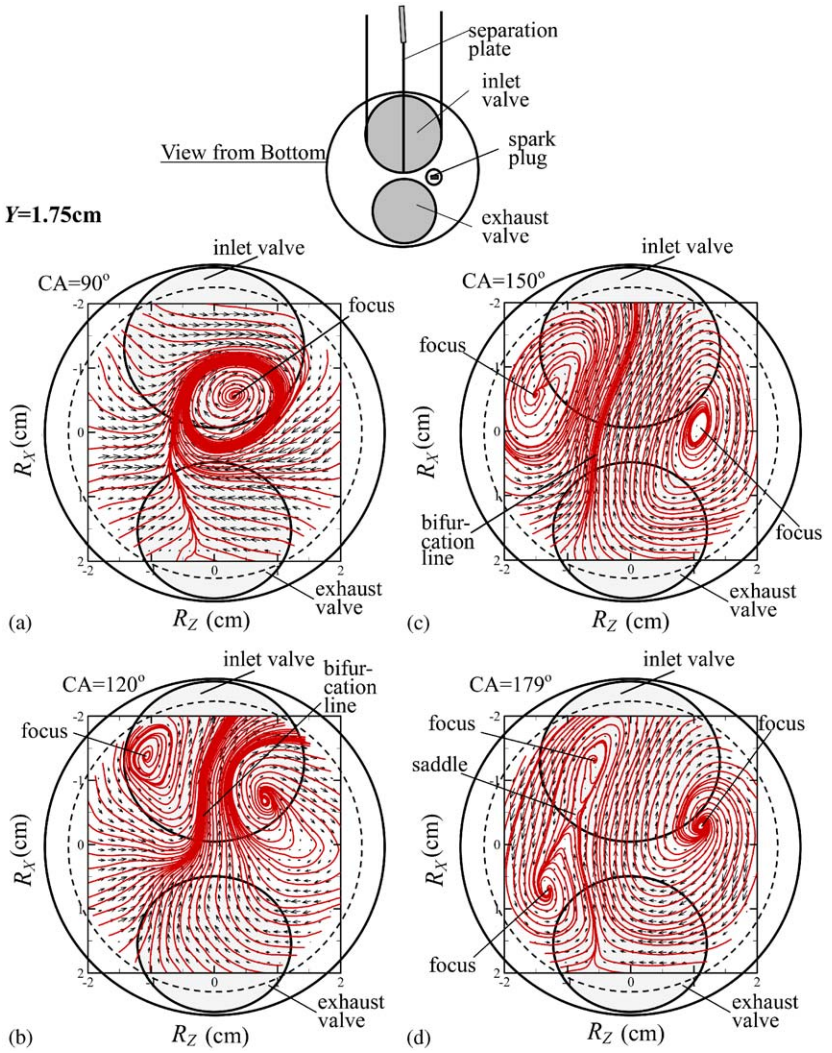

Fig. 11. Evolution of swirl flow motions during intake stroke in diametral plane $Y = 1.75$ cm. Inlet deflection-valve fully open ($\Phi = 83^\circ$). Engine speed $N = 1500$ rpm. Velocity data are ensemble-averaged from 100 instantaneous measurements.

(Tritton, 1988) because the flow is a little unbalanced about the symmetry plane. A "four-way saddle" located at $(X, Y) \approx (4, 2.2)$ cm is induced subsequently to satisfy the topological rule (Hunt et al., 1978) because of the formation of the unstable focus. There are two "positive open bifurcation lines": one evolves from the unstable focus towards the four-way saddle and the other evolves from the right upper corner towards the four-way saddle. In the region above these two bifurcation lines, the flow points upward because of the effect induced by the bluff-body wake. Below these bifurcation lines, the flow goes downward and turns left due to the downward motion of the piston. The influence of the jet flow going through the left part of the inlet valve is different from that in Fig. 5(b): the reverse flow going toward the inlet valve turns to the left, merges with the flow coming from the left part of the valve, then forms a clockwise-rotating vortex around the left-upper corner of Fig. 7(b). This flow pattern evolves with the increase of the crank angle.

At CA = 150°, as shown in Fig. 7(c), the "unstable focus" in Fig. 7(b) moves downward with the downward motion of the piston and is out of sight of the PIV view-window. The "saddle point" in Fig. 7(b) disappears and the "positive open bifurcation line" elongates toward right-upper corner. To the right of the "positive open bifurcation line", a clockwise-rotating vortex is formed. To the left of the bifurcation line, the flow goes upward. Around the left-upper corner, the clockwise-rotating vortex enlarges and the vortex center is obvious. This typical flow pattern lasts to the end of the intake stroke, as shown in Fig. 7(d).

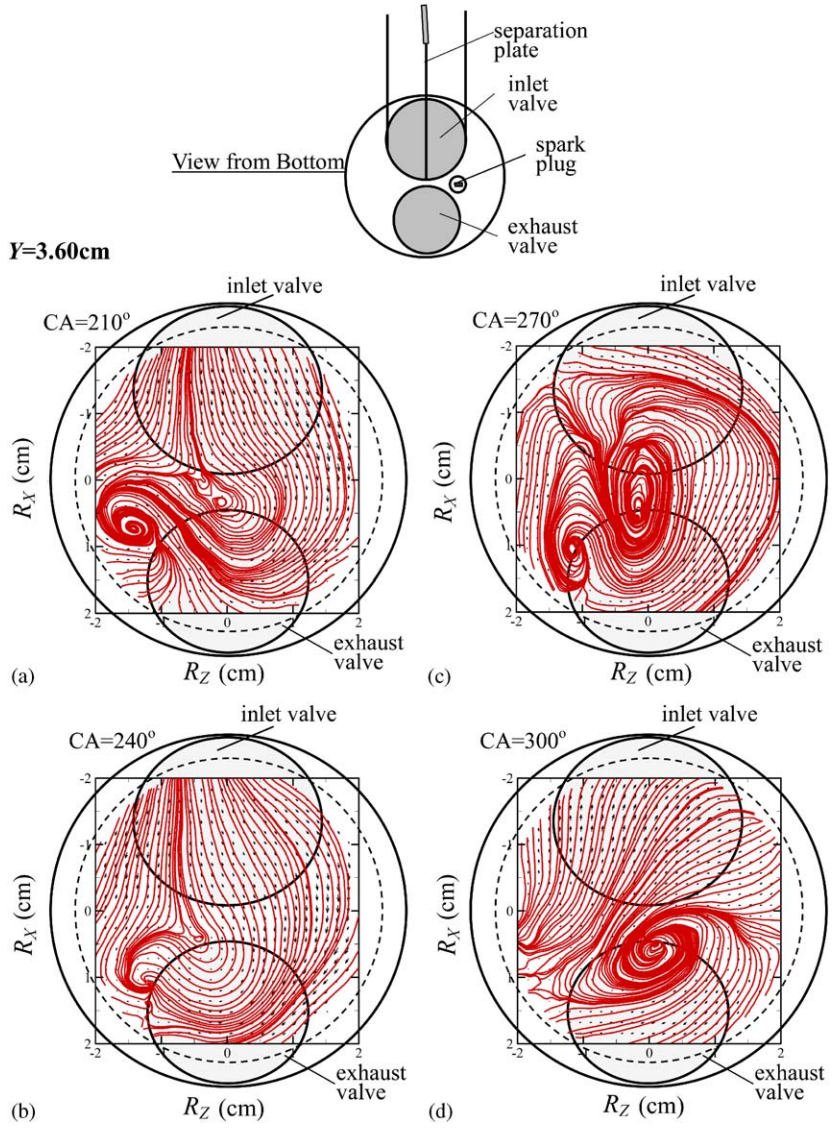

Fig. 12. Evolution of swirl flow motions during compression stroke in diametral plane $Y = 3.6$ cm. Inlet deflection-valve fully open ($\Phi = 83^\circ$). Engine speed $N = 1500$ rpm. Velocity data are ensemble-averaged from 100 instantaneous measurements.

In the compression stroke, as shown in Fig. 8, the clockwise-rotating vortices around the left-upper and the right-lower corners all disappear. Instead, flows in the cylinder are dominated by upward flows.

3.2. Flow evolution in diametral plane

3.2.1. Inlet deflection-valve closed ($\Phi = 0^\circ$)

Fig. 9 shows the evolution process of the in-cylinder flows in the plane of $Y = 1.75$ cm during intake stroke. The inlet deflection-valve is closed ($\Phi = 0^\circ$), so that the inlet stream is drastically deflected by the deflection-valve. When the inlet valve is open, the air is drawn by the downward moving piston. It passes over the inlet valve, and forms an annular jet in the cylinder. Because the annular jet is significantly unbalanced by the deflection-valve, an asymmetric flow pattern in the diametral plane is expected. As shown in Fig. 9(a) for CA = 90°, most flow comes out of the left part of the inlet-valve opening, so that a flow region with counter-clockwise-rotating tendency occupies a large portion in the left of the diametral plane. Separated by a "negative open bifurcation line", a small flow region with clockwise-rotating vortex

exists in the right part of the plane. As the piston goes further downward, the vortex-stretching effect in $-Y$ direction alters the flow structure in this diametral plane gradually: the intensities of the left and right vortices increase and the relative positions shift at CA = 120° (Fig. 9(b)), the left vortex enlarges and is enhanced at CA = 150° (Fig. 9(c)), and finally at the end of intake stroke most of the diametral plane is occupied by the counter-clockwise-rotating vortex centering about an "unstable focus" (Fig. 9(d)). The formation of a vortex around a focus and the increase of vorticity are natural when the flow in a cylinder is subject to an axial stretch (Tritton, 1988; Tennekes and Lumley, 1972). Only a very small region in the right-lower corner has traces of low-intensity clockwise-rotating vectors. The conventionally called "swirl motion" is established.

Fig. 10 shows the evolution process of the in-cylinder flows in the diametral plane of $Y = 3.6$ cm during compression stroke. In the diametral plane located at upper-level of the cylinder, which is not shown here, the single clockwise-rotating large-scale swirl motion is still not established at the end of the intake stroke, because the stretching effect in $-Y$ direction is strong in the lower-lever region near the downward moving piston head and is weak in the higher-level region. Two unequal-size counter-rotating vortices separated by a "negative open bifurcation line" do exist. The two vortices evolve when the compression process proceeds, as shown in the sequence of Figs. 10(a)–(d) for crank angle increasing from CA = 210° to 300°. The counter-clockwise-rotating vortex on the left side enlarges first when the crank angle is increased to CA = 240°, as shown in Fig. 10(b), then expands to almost the whole diametral plane centering around an "unstable focus", as shown in Fig. 10(c) for CA = 270°. In this upper-level plane, the "swirl motion" is established in the compression stroke, instead of in the intake stroke as has been shown in Fig. 9(d) for the lower-level plane.

3.2.2. *Inlet deflection-valve fully open ($\Phi = 83°$)*

Fig. 11 shows the evolution process of the flows in the diametral plane $Y = 1.75$ cm during the intake stroke when the inlet deflection-valve is fully open. Because the deflection-valve is 3° deviated from the central plane of the inlet passage, as described in a previous section, the inlet flow is a little deflected (the flow going through the right passage is a little more than that going through the left passage), the slightly unbalanced inlet flow spreads out of the valve gap and induces a specific flow pattern as shown in Fig. 11(a). In the right-lower region, the flow goes to the left; while in the left-lower region, the flow goes to the right and therefore forms a "negative open bifurcation line". In the right-upper region, a clockwise-rotating vortex is established by centering about a "unstable focus". The vortex in Fig. 11(a) enlarges by the effect of vortex-stretching in $-Z$ direction, which is induced by the downward motion of the piston as the crank angle increases. However, a complete swirl motion in the whole diametral plane is still not established until the end of the intake stroke (Figs. 11(b), (c) and (d)). In Fig. 11(d), a large clockwise-rotating vortex occupies about two-thirds of the view circle. The rotation direction is opposite to that in Fig. 9(d), because the deflection directions in these two cases are opposite.

The complete swirl vortex is not observed throughout the compression stroke, as shown in Figs. 12(a)–(d). The evolution process is completely different from the case in which the inlet flow is significantly deflected.

3.3. *Quantitative analysis of in-cylinder flow motions*

In order to quantify the above mentioned flow motions in the symmetry and diametral planes, a tumble ratio ($T_{v,CA}$) and a swirl ratio ($S_{v,CA}$) at certain crank angle (Rouland et al., 1998) are defined as follows:

$$T_{v,CA} = \frac{\sum_{i=1}^{n} \left(\frac{\partial v}{\partial X} - \frac{\partial u}{\partial Y} \right)_i}{2n\omega}, \tag{1}$$

$$S_{v,CA} = \frac{\sum_{i=1}^{n} \left(\frac{\partial u}{\partial R_Z} - \frac{\partial w}{\partial R_X} \right)_i}{2n\omega}, \tag{2}$$

where $((\partial v/\partial X) - (\partial u/\partial Y))$ and $((\partial u/\partial R_X) - (\partial w/\partial R_Z))$ are vorticities for tumble ratio and swirl ratio, respectively, the subscript i stands for the number of grids set up for the data-points in the target plane, n is the total number of grid points, and ω is the crank shaft angular speed in radians per second which can be calculated by $\omega = 2\pi N/60$ (N is the engine speed in rpm). In conducting calculations of the vorticity, central difference scheme is applied at each grid point. The numerator in Eqs. (1) and (2) represents the total amount of large and small-scale rotations in the target plane. For a rotating rigid body, vorticity has a constant value equal to twice the angular velocity. Therefore, the tumble ratio, $T_{v,CA}$, and the swirl ratio, $S_{v,CA}$, can be interpreted as the ratio of the mean angular velocity of the vortices in the target plane at a certain crank angle which is divided by average crank angle velocity.

3.3.1. Tumble ratio

Fig. 13 shows the variation of the tumble ratio $T_{v,CA}$ with the inlet deflection-valve open angle Φ at various crank angles. During the intake stroke (Fig. 13(a)), the tumble ratios at crank angle CA = 60° and 90° are very low for all open angles of the inlet deflection-valve. Because the clockwise-rotating large vortex in the symmetry plane is apparently developed only when CA > 90°, as has been illustrated in Figs. 5(b)–(d), the tumble ratios at CA > 90° are negatively larger than those at CA < 90°. The tumble intensities are negatively the largest when the inlet stream is completely deflected ($\Phi = 0°$). The magnitude of $T_{v,CA}$ decreases rapidly when Φ increases from 0° to 40°. For $\Phi > 40°$, the increase rate becomes imperceptible, which is in accordance with the flow pattern evolutions shown in Fig. 7. The inlet flow deflection is beneficial to the formation of a tumble structure in the symmetry plane, particularly at $\Phi < 40°$. During the compression stroke, as shown in Fig. 13(b), the tumble ratio decreases with the evolution of the crank angle, which is correlated with the flow-pattern evolutions shown in Figs. 6 and 8. During the later period of the compression

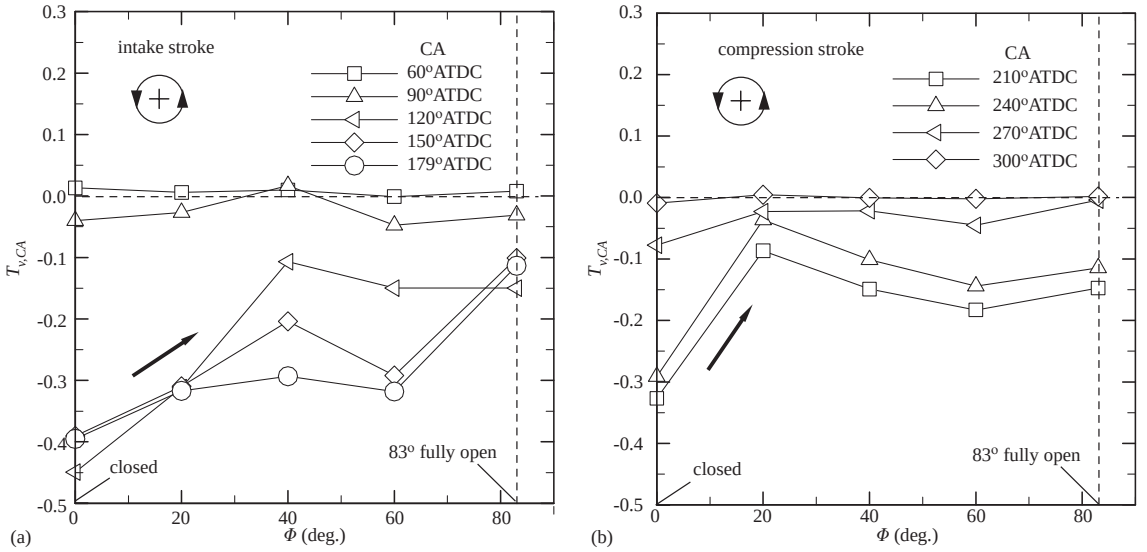

Fig. 13. Variation of tumble ratio with angle of inlet deflection-valve. (a) Intake stroke, (b) compression stroke.

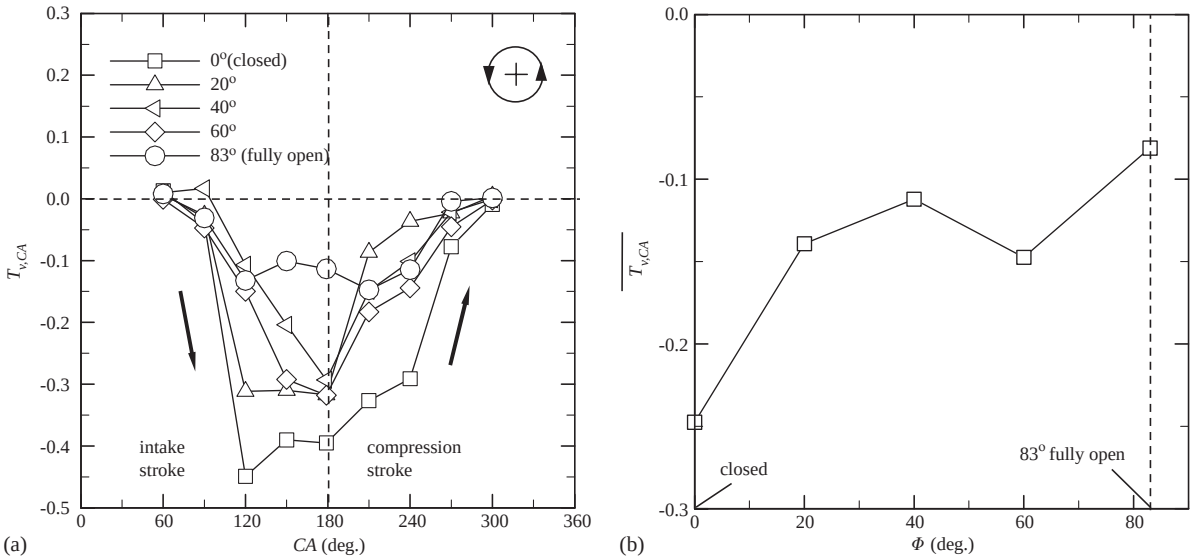

Fig. 14. (a) Variation of tumble ratio with crank angle, (b) cycle-averaged tumble ratio.

stroke, e.g., CA > 270°, the tumble intensity becomes negligibly small for all inlet deflection angles because of the effect of vortex compression in the axial direction and the shortage of supply air. During the first-half of the compression stroke, the tumble intensity remains negatively large when the angle of the inlet deflection valve is smaller than 20°. In other words, the tumble motion developed during the intake stroke can last to the first half-period of compression stroke before it disappears.

The variation of the tumble ratio with the crank angle can be observed more clearly in Fig. 14(a). For all inlet deflection angles, magnitude of $T_{v,CA}$ increases significantly with the downward motion of the piston. When the crank angles are smaller than 60°, the tumble ratios are negligibly small. Appreciably large tumble motion is established in the intake stroke of engine operation when the piston moves downward to about CA = 120°. The magnitudes of $T_{v,CA}$ attain the maximum values for CA = 120°−180°, then decrease progressively when the compression is increased. The tumble structure remains evolving and lasts in the compression stroke when the piston moves upward to about CA = 240°. After CA = 240°, the tumble intensity disappears rapidly. The tumble intensity becomes almost null when the crank angle is greater than 300°. If the tumble ratio $T_{v,CA}$ in Fig. 14(a) is integrated over the crank angle from the intake through the compression strokes and normalized by the crank angle period of integration, a cycle-averaged tumble ratio $\overline{T_{v,CA}}$ can be calculated and is presented in Fig. 14(b) for various Φ. Obviously, the cycle-averaged tumble ratio in the symmetry plane is extraordinarily large when the inlet stream is significantly deflected, e.g. $\Phi < 20°$.

3.3.2. Swirl ratio

As shown in Fig. 15(a), during the intake stroke the swirl ratio $S_{v,CA}$ increases with the increase of crank angle. During the compression stroke, as shown in Fig. 15(b), the swirl ratios for $\Phi \geqslant 40°$ are negligibly small and do not vary with the increase of the crank angle. For $\Phi < 40°$, where the inlet flows are significantly deflected, the swirl ratios remain high and increase with the increase of crank angle until CA = 270°, then decay a little gradually to the final stage of the compression process. Figs. 15(c) and (d) show variations of the swirl ratio with the inlet deflection angle during intake and compression strokes, respectively. In Fig. 15(c) for the intake stroke, at each crank angle the swirl ratio are high at $\Phi < 40°$ and decreases rapidly with the increase of Φ. In Fig. 15(d) for the compression stroke, the situation is similar to

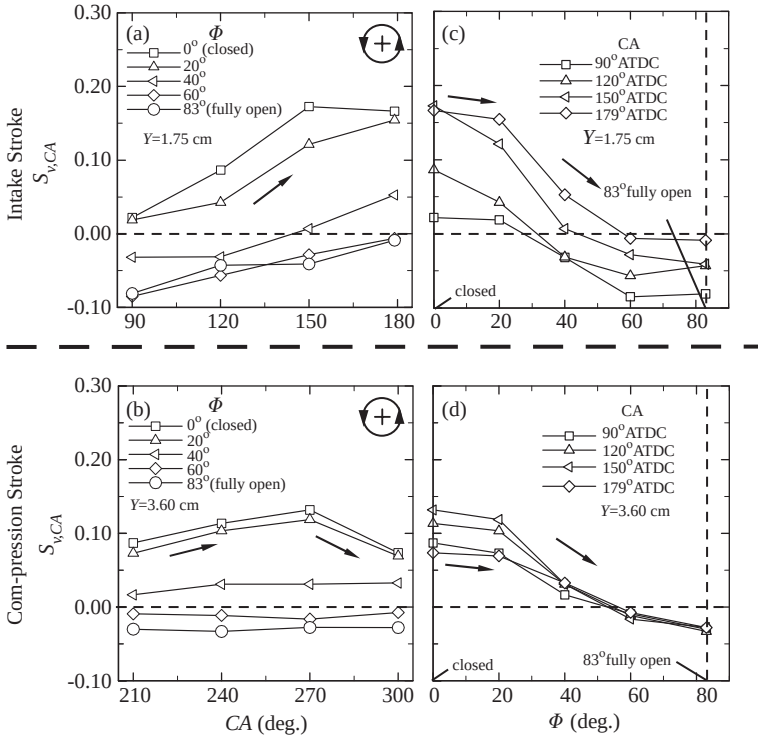

Fig. 15. Variation of swirl ratio with crank angle (a, b), and with angle of inlet deflection-valve (c,d); (a,c) for intake stroke, (b,d) for compression stroke.

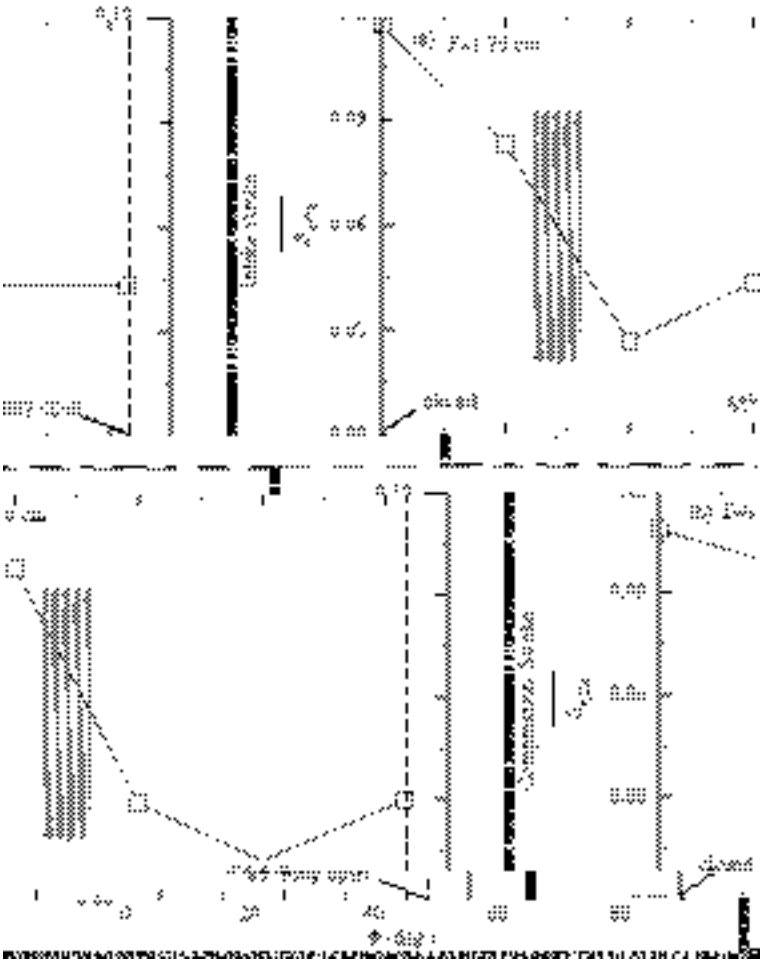

Fig. 16. Variation of cycle-averaged swirl ratio with angle of inlet deflection-valve.

what occurs in Fig. 15(c). Therefore, it is obvious that by deflecting the inlet stream at $\Phi<40^\circ$ (significantly blocking one side of the inlet passage), swirl strength can be gained, and the swirl ratio remains high for a long period, even to the final stage of the compression stroke.

If the swirl ratio $S_{v,CA}$ in Figs. 15(c) and (d) are integrated over the crank angle for each Φ and normalized by the crank angle period of integration, a cycle-averaged swirl ratio $\overline{S_{v,CA}}$ can be calculated for intake and compression, as shown in Figs. 16(a) and (b), respectively. Obviously, the cycle-averaged tumble ratio in the diametral plane is large at $\Phi<40^\circ$, at which the inlet stream is drastically deflected. When the swirl and/or the tumble ratios are promoted, the mixing induced by the large-scale rotating flow motions and the small-scale turbulent eddy convection are expected to be significant (Ekchian and Hoult, 1979; Hirotomi et al., 1981; Arcoumanis et al., 1982; Liou and Santavicca, 1985; Nadarajah et al., 1998).

3.4. Correlation with engine performance

In order to establish the correlation between the flow motions and the engine performance, the engine is hooked up to a test rig and driven by an eddy-current dynamometer (type Tokyokoki-Schenck W-40) via two rubber couplings and a homemade driveshaft. The maximum hose power, torque, and speed of the dynamometer are 60 PS, 7.612 kg m, and 17 000 rpm, respectively. The load cell is model SSN-AJ-500N made by Interface Co. In the test rig, the specific fuel consumption (fuel consumption rate divided by the engine power) and various exhaust concentrations are also measured by proper instruments.

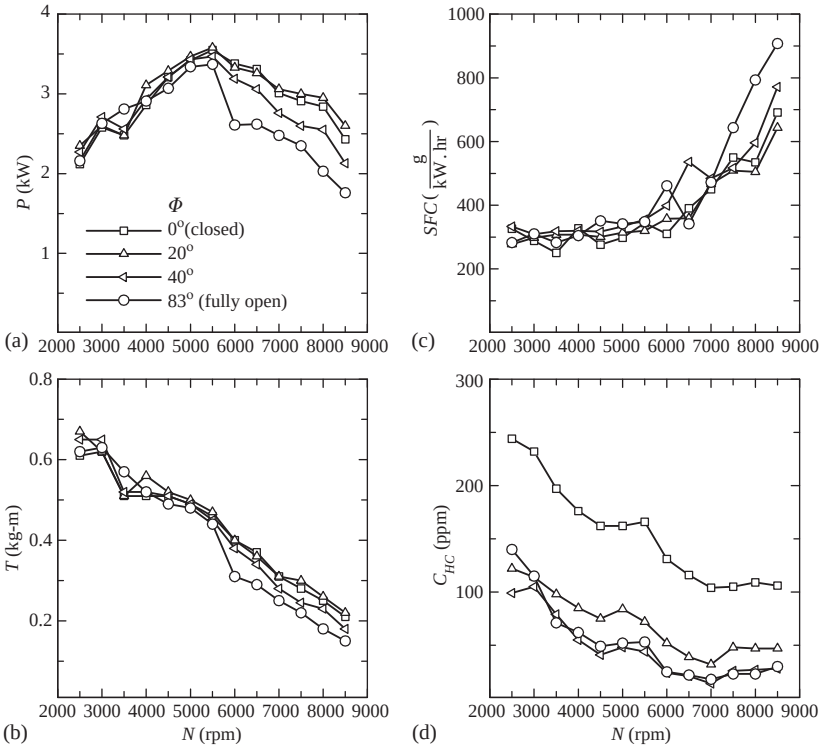

Fig. 17. Engine performance at throttle opening 25%: (a) power, (b) torque, (c) specific fuel consumption, (d) concentration of hydrocarbons in the exhaust.

The power P, torque T, specific fuel consumption SFC, and concentration of hydrocarbonC_{HC} measured at standard dynamometer engine test rig with 25% opening of the throttle are shown in Fig. 17. Compared with the test results of $\Phi = 83^\circ$ (inlet deflection-valve fully open), it is apparent that the engine power P and the torque T are raised when the inlet deflection is applied, particularly at large deflection angles of $\Phi < 40^\circ$. The specific fuel consumption SFC has the reverse effect. The inlet-stream deflected engine provides better (less) fuel consumption rate than the inlet-stream undeflected engine. However, the concentrations of hydrocarbon pollutants of the inlet stream-deflected engines are worse when compared with the undeflected one, particularly when the deflection is the largest, i.e., $\Phi = 0^\circ$. When the engine is operated at the throttle opening smaller than about 40%, all of the measured engine performances are similar to those shown in Fig. 17. It implies that if one is interested in the common operation situation in an urban area, e.g., while idling or for low throttle drive, applying the inlet-stream deflection may be beneficial for power, torque, and fuel consumption. However, heavy deflection, e.g., $\Phi = 0^\circ$, has a negative effect on the exhaust pollutants.

The power, torque, specific fuel consumption, and concentration of hydrocarbons measured by a standard dynamometer engine test rig with 50% opening of throttle are shown in Fig. 18. Compared with the test results of $\Phi = 83^\circ$ (fully open), the engine power P and torque T are lowered when the inlet deflection is applied, particularly at the large deflection angle of $\Phi < 40^\circ$. The specific fuel consumption SFC and the hydrocarbon concentration C_{HC} are not significantly influenced by the deflection of inlet stream. When the engine is operated at throttle opening larger than about 40%, the engine performances are similar to those shown in Fig. 18.

At large throttle openings, the blockage of the inlet passage induced by the inlet-deflection valve may cause significant decrease in the charge efficiency. Under this situation, the negative effect of insufficient inlet flow on the engine performance overwhelms the positive effect of the enhanced swirl and the tumble motions induced by the deflection of inlet stream. The charge efficiency thus dominates the engine performance at large throttle-opening operations. However, at smaller throttle-opening operations, the percentage deterioration of the charge efficiency is not as large as what is encountered in the case of large throttle opening. Therefore, the benefits gained from the enhanced swirl and tumble motions may overwhelm the negative effect induced by the decrease of the charge efficiency.

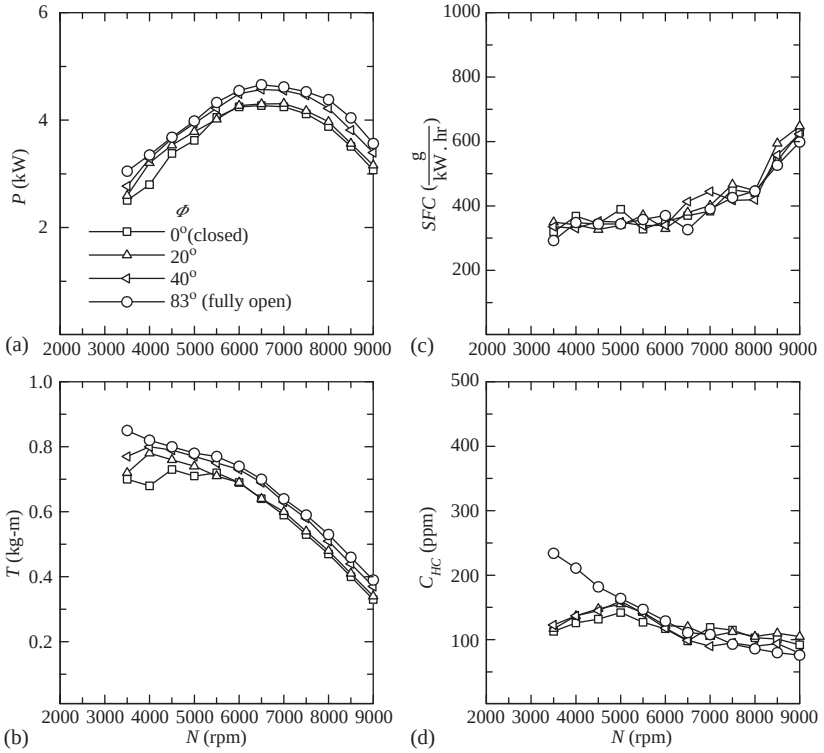

Fig. 18. Engine performance at throttle opening 50%: (a) power, (b) torque, (c) specific fuel consumption, (d) concentration of hydrocarbons in the exhaust.

5. Conclusions

The evolution processes of the in-cylinder tumble and the swirl flows of a motored two-valve, single cylinder, four stroke engine with/without inlet-stream deflection during the intake and compression strokes are diagnosed by using a PIV. By employing the quantified nondimensional parameters, the correlation between the in-cylinder flow motions and the engine performance is also established. The conclusions listed below are drawn from the results and discussion.

(i) When the inlet stream is deflected drastically, an apparent tumbling vortical flow structure in the symmetry axial plane would be established during the intake stroke as the piston is going downward and passing halfway through the intake stroke. The strength of the tumble motion attains maximum between crank angles of 120° and 180° and decays progressively in the compression stroke with increasing crank angle, until it diminishes after the piston passes through halfway of the compression stroke. Without inlet-stream deflection, the tumble motion in the symmetry axial plane is insignificant throughout the cycle. This explains why the currently delivered commercial engines prefer four or more intake valves to generate strong tumble flows instead of using a two-vale configuration.

(ii) When the inlet stream is deflected drastically, apparent swirl motion in the symmetry axial plane would be established during the intake stroke. A complete swirling vortical flow structure occupying the whole diametral plane occurs at the final stage of the intake stroke. The strength of the swirl motion increases with the increase of the crank angle and attains maximum as the piston is going downward and passing halfway through the intake stroke. The strength of the swirl motion keeps increasing during the first half of the compression stroke and decays successively. Without inlet-stream deflection, the complete swirling vortical flow structure would never be found throughout the cycle.

(iii) When the engine is operated at a throttle opening smaller than about 40%, applying the inlet-stream deflection would increase engine power and torque, and decrease the specific fuel consumption. However, the concentrations of the hydrocarbon in the exhaust become worse, particularly when the deflection is very large. When the engine is operated at the throttle opening larger than about 40%, a drastic decrease of the charge efficiency dominates the engine performance. Under this situation the inlet-stream deflected flows do not have enough merit in enhancing

the mixing and flame propagation. Inversely, the pressure is drastically reduced, so that the charge efficiency is low. Therefore, the engine performance is impaired.

Acknowledgments

This research was granted and supported by the Kymco Industry of Taiwan. Assistance from Mr M.L. Tsai and Mr H.Y. Hsu of the Kymco Industry in modifying the engine parts are appreciated.

References

Adrian, R., 1991. Particle-imaging techniques for experimental fluid mechanics. Annual Review of Fluid Mechanics 23, 261–304.

Arcoumanis, C., Bicen, A.F., Vlachos, N.S., Whitelaw, J.H., 1982. Effects of flow and geometry boundary conditions on fluid motion in a motored IC model engine. Proceedings of the Institution of Mechanical Engineers 196, 1–10.

Arcoumanis, C., Godwin, S.N., Kim, J.W., 1998. Effect of tumble strength on combustion and exhaust emissions in a single-cylinder, four-valve, spark-ignition engine. SAE paper 981044, Warrendale, PA, USA.

Cao, Z.-M., Nishino, K., Mizuno, K., Torii, K., 2000. PIV measurement of internal structure of diesel fuel spray. Experiments in Fluids (Suppl.), S211–S219.

Chong, M.S., Perry, A.E., 1990. A general classification of three-dimensional flow fields. Physics of Fluids A 2, 765–777.

Ekchian A., Hoult, D.P., 1979. Flow visualization study of the intake process of an internal combustion engine. SAE paper 790095, Warrendale, PA, USA.

Freek, C., Hentschel, W., Merzkich, W., 1998. High speed PIV—a diagnostic tool for IC-engines. Proceedings of the Eighth International Symposium on Flow Visualization, pp. 185.1–185.10.

Glass, M., Kennedy, I.M., 1978. An improved seeding method for high temperature laser-Doppler velocimetry. Combustion & Flame 29, 333–335.

Hart, D.P., 1999. Super-resolution PIV by recursive local-correlation. Journal of Visualization 10, 1–10.

Heywood, J.B., 1987. Fluid motion within the cylinder of internal combustion engines. ASME Journal of Fluids Engineering 109, 3–35.

Heywood, J.B., 1988. Internal Combustion Engine Fundamentals. McGraw-Hill, New York.

Hirotomi, T., Nagayama, I., Kobayashi, S., Yamamasu, T., 1981. Study of induction swirl in a spark ignition engine. SAE paper 810496, Warrendale, PA, USA.

Huang, R.F., Lin, C.L., 1994. Visualized flow patterns of double concentric jets at low annulus velocities. AIAA Journal 32, 1868–1874.

Huang, R.F., Lin, C.L., 1997. Flow characteristics and shear-layer vortex shedding of double concentric jets. AIAA Journal 35, 887–892.

Huang, R.F., Tsai, F.C., 2001a. Observation of swirling flows behind circular discs. AIAA Journal 39, 1106–1112.

Huang, R.F., Tsai, F.C., 2001b. Flow field characteristics of swirling double concentric jets. Experimental Thermal and Fluid Science 25, 151–161.

Huang, R.F., Yen, S.C., 2003. Axisymmetric swirling vortical wakes modulated by a control disk. AIAA Journal 41, 888–896.

Hunt, J.C.R., Abell, C.J., Peterka, J.A., Woo, H., 1978. Kinematical studies of the flows around free or surface-mounted obstacles; applying topology to flow visualization. Journal of Fluid Mechanics 86, 299–446.

Iwamoto, Y., Noma, K., Nakayama, O., Yamauchi, T., Ando, H., 1997. Development of gasoline direct injection engine. SAE paper 970541, Warrendale, PA, USA.

Jackson, N.S., Stokes, J., Sadler, M., Heikal, M.R., Faure, M., Pommier, L., 1997. Correlation of the combustion characteristics of spark ignition engines with the in-cylinder flow field characterized by PIV in a water analogy rig. SAE paper 971637.

Keane, R.D., Adrian, R.J., 1990. Optimization of particle image velocimeters, Part I: Double pulsed systems. Measurement Science and Technology 1, 1202–1215.

Keane, R.D., Adrian, R.J., 1992. Theory of cross-correlation analysis of PIV images. Applied Scientific Research 49, 191–215.

Keane, R.D., Adrian, R.J., Zhang, Y., 1995. Super-resolution particle imaging velocimetry. Measurement Science and Technology 6, 754–768.

Khalighi, B., 1991. Study of the intake tumble motion by flow visualization and particle tracking velocimetry. Experiments in Fluids 10, 230–236.

Lee, J., Farrel, P.V., 1993. Intake valve flow measurements of an IC engine using particle image velocimetry. SAE paper 930480, Warrendale, PA, USA.

Liou, T.-M., Santavicca, D.A., 1985. Cycle resolved LDV measurements in a motored IC engine. ASME Journal of Fluids Engineering 107, 232–240.

Mei, R., 1996. Velocity fidelity of flow tracer particles. Experiments in Fluid 22, 1–13.

Nadarajah, S., Balabani, S., Tindal, M.J., Yianneskis, M., 1998. The effect of swirl on the annular flow past an axisymmetric poppet valve. Proceedings of the Institution of Mechanical Engineers, Part C, 212, 473–484.

Perry, A.E., Fairlie, B.D., 1974. Critical points in flow patterns. Advances in Geophysics B 18, 299–315.
Raffer, M., Willert, C.E., Kompenhans, J., 1998. Particle Image Velocimetry—A Practical Guide. Springer, Berlin.
Rask, R.B., 1979. Laser Doppler anemometer measurements in an internal combustion engine. SAE paper 790094, Warrendale, PA, USA.
Rouland, E., Floch, A., Ahmed, A., Dionnet, D., Trinite, M., 1998. Characterization of intake generated tumble flow in 4-valve engine using cross-correlation particle image velocimetry. Proceedings of the Eighth International Symposium on Flow Visualization, pp. 195.1–195.15.
Tennekes, H., Lumley, J.L., 1972. A First Course in Turbulence. MIT Press, Cambridge.
Tritton, D.J., 1988. Physical Fluid Dynamics. Oxford University Press, Oxford.
Valentino, G., Kaufman, D., Farrel, P.V., 1993. Intake valve flow measurements using PIV. SAE paper 932700, Warrendale, PA, USA.